ADVANCED MATERIALS
www.advmat.de

Bitter Flavored, Soft Composites for Wearables Designed to Reduce Risks of Choking in Infants

Donghwi Cho, Rui Li, Hyoyoung Jeong, Shupeng Li, Changsheng Wu, Andreas Tzavelis, Seonggwang Yoo, Sung Soo Kwak, Yonggang Huang, and John A. Rogers**

Wireless, skin-integrated devices for continuous, clinical-quality monitoring of vital signs have the potential to greatly improve the care of patients in neonatal and pediatric intensive-care units. These same technologies can also be used in the home, across a broad spectrum of ages, from beginning to end of life. Although miniaturized forms of such devices minimize patient burden and improve compliance, they represent life-threatening choking hazards for infants. A materials strategy is presented here to address this concern. Specifically, composite materials are introduced as soft encapsulating layers and gentle adhesives that release chemical compounds designed to elicit an intense bitter taste when placed in the mouth. Reflexive reactions to this sensation strongly reduce the potential for ingestion, as a safety feature. The materials systems described involve a non-toxic bitterant (denatonium benzoate) as a dopant in an elastomeric (poly(dimethylsiloxane)) or hydrogel matrix. Experimental and computational studies of these composite materials and the kinetics of release of the bitterant define the key properties. Incorporation into various wireless skin-integrated sensors demonstrates their utility in functional systems. This simple strategy offers valuable protective capabilities, with broad practical relevance to the welfare of children monitored with wearable devices.

1. Introduction

The COVID-19 pandemic has greatly increased an appreciation for the value of continuous, digital tracking of health status, in the hospital, in managed care facilities, in the home, and in the workplace.[1] Technologies for vital signs monitoring in intensive care units (ICUs) define the "gold standard" for real-time, precise assessments.[2] The strong adhesives and wired based interfaces associated with these systems,[3,4] however, lead to significant complications for even basic aspects of care, they create irritation at the skin interface and they impose other physical and mechanical constraints, particularly problematic for patients in neonatal intensive care units (NICUs) and pediatric intensive care units (PICUs).[5–7] Recent efforts in soft electronics establish the basis for wireless, skin-interfaced devices that are capable of non-invasive, continuous monitoring with clinical-grade

Dr. D. Cho, Dr. H. Jeong, Dr. C. Wu, A. Tzavelis, Dr. S. Yoo, Dr. S. S. Kwak, J. A. Rogers
Querrey Simpson Institute for Bioelectronics
Northwestern University
Evanston, IL 60208, USA
E-mail: jrogers@northwestern.edu

Prof. R. Li
State Key Laboratory of Structural Analysis for Industrial Equipment
Department of Engineering Mechanics
Dalian University of Technology
Dalian 116024, China

Prof. R. Li
International Research Center for Computational Mechanics
Dalian University of Technology
Dalian 116024, China

S. Li, Prof. Y. Huang
Department of Mechanical Engineering
Northwestern University
Evanston, IL 60208, USA
E-mail: y-huang@northwestern.edu

The ORCID identification number(s) for the author(s) of this article can be found under https://doi.org/10.1002/adma.202103857.

S. Li, Prof. Y. Huang
Department of Civil and Environmental Engineering
Northwestern University
Evanston, IL 60208, USA

S. Li, Prof. Y. Huang
Department of Materials Science and Engineering
Northwestern University
Evanston, IL 60208, USA

A. Tzavelis
Medical Scientist Training Program
Feinberg School of Medicine
Northwestern University
Chicago, IL 60611, USA

A. Tzavelis, Prof. J. A. Rogers
Department of Biomedical Engineering
Northwestern University
Evanston, IL 60208, USA

Dr. S. S. Kwak
School of Advanced Materials Science and Engineering
Sungkyunkwan University (SKKU)
Suwon 16419, Republic of Korea

DOI: 10.1002/adma.202103857

accuracy, in nearly any environment and during natural daily activities.[8–10] These miniature sensors, which gently adhere to the skin and impose minimal burden on patients, offer the greatest benefits for infants. A serious concern for use with this population, however, follows from risks of choking or blocking of the gastrointestinal (GI) tract following accidental ingestion.[11–15]

Materials oriented strategies have the potential to minimize such types of risks, as demonstrated in certain types of batteries[16] and gaming devices.[17] Here, bitter tasting substances applied as thin coatings on these objects elicit strong reflexive reactions when placed in the mouth, with proven ability to reduce the potential for ingestion.[18] Inspired by these strategies, we introduce classes of soft composite materials as encapsulating structures and adhesive layers for wireless, skin-interfaced devices designed to monitor vital signs. These materials exploit denatonium benzoate (DB), the most bitter substance known to pose little or no hazard to human health,[18,19] dispersed in matrices of poly(dimethylsiloxane) (PDMS) or hydrogel. Experimental measurements and diffusion modeling define the kinetics of release of the DB upon exposure to water. Demonstrations with various wireless, skin-integrated devices highlight some practical application possibilities.

2. Results and Discussion

2.1. Material Designs for the Bitter Flavored Elastomer Composites

Figure 1 summarizes the key materials concepts for a bitter flavored elastomer composite formed by planetary mixing of the bitterant additive DB (bitterness threshold of 0.05 parts-per-million)[20] into a prepolymer to PDMS. A typical formulation of this DB-PDMS material includes a small quantity (≈1 wt%) of fine DB powders formed by pre-ball milling and sieving through a fine mesh (average diameter of 45 μm). Curing of the PDMS involves hydrosilylation reactions that create crosslinks between silicon hydride and vinyl siloxane groups, catalyzed by a platinum complex (Pt).[21–23] This Pt catalyst can be readily deactivated by chelating functional groups such as the amino group in DB.[22,24] As a result, this type of composite involves some spatial heterogeneity in the crosslinking density, as illustrated schematically in Figure 1a,b. Specifically, the PDMS polymer chains near the microparticles of DB are depleted in Pt catalyst due to the chelating effect and therefore have a reduced density of crosslinks.[22] The results of swelling/deswelling tests with cyclohexane provide indirect evidence of loosely or uncrosslinked polymer chains in DB-PDMS and corresponding reductions in the density of the crosslinked network (Figure S1, Supporting Information). Compared to PDMS, during the swelling, the DB-PDMS exhibits a significant increase in weight due to enhanced solvent permeation through less crosslinked regions of the composite. The weight ratio (weight of swollen sample/weight of original sample) increases up to 3.76 for the DB-PDMS with 1.0 wt%, which is ≈100% higher than that measured with undoped PDMS (ratio of 1.88) formed at the same mixing ratio of silicone oligomer and curing agent (10:1). After drying and deswelling, the DB-PDMS (1.0 wt%) has a weight lower than the original value due to the extraction of polymer chains from the loosely or uncrosslinked regions.[22] (DB is insoluble in cyclohexane.) The net effects of the DB and its influence on crosslinking are to increase the mechanical compliance of the material[25,26] and improve its conformality and adhesion to the skin (Figure 1c).

As shown in Figure 1d, DB particles at and near the surface of the composite readily dissolve and diffuse into surrounding water, due to their high water solubility (42 400 mg L^{-1} at 20 °C).[27] This process leaves microscale pores near the surface and releases bitterant. Figure 1e,f illustrates the result for the application envisioned here.

2.2. Effect of DB Doping on the Optical and Mechanical Properties of Silicone and Hydrogel Composites

Figure 2a shows the dependence of the optical properties of films of DB-PDMS (thicknesses of 500 μm) on DB concentration up to 1.0 wt%. The films become increasingly opaque with doping due to scattering that arises from regions of DB (refractive index ≈ 1.58) within the PDMS (refractive index ≈ 1.43) matrix (Figure S2, Supporting Information).[28,29] Measurements with an integrating sphere indicate that UV absorption associated with DB[30] increases the absorbance in this wavelength range as the loading ratio increases (Figure 2a and Figure S3: Supporting Information).

As mentioned previously, the chelating effect of the DB on the Pt catalyst reduces the crosslinking density locally near the DB microparticles, with dramatic implications for the mechanical properties.[22] The stress-strain behaviors of composites with DB concentrations up to 1.0 wt% appear in Figure 2b, for strains up to 50%, comparable to the maximum values for natural motions of the skin.[31] For the 1.0 wt% case, the Young's modulus of the composite is ≈173 kPa, corresponding to a significant reduction from the value (≈1 MPa) for pure PDMS (mixed with a weight ratio of 10 to 1, monomer to crosslinking agent). Figure 2c summarizes rheological measurements of the viscoelastic properties in terms of the storage G' and loss G'' moduli as a function of frequency from 10^{-2} to 10^{2} Hz. The similar frequency dependence for G' of the doped and undoped cases suggests similar levels of entanglement for the densely crosslinked networks in both materials.[22] The reduced density of crosslinks in the DB-PDMS, however, leads to decreases in both G' and G'' across the frequency range. In particular, the reductions in G'' are most significant at low frequencies (0.01 to 1 Hz), consistent with some level of viscous flow in the heterogeneously crosslinked network.[22]

Prof. J. A. Rogers
Department of Chemistry
Northwestern University
Evanston, IL 60208, USA
Prof. J. A. Rogers
Department of Neurological Surgery
Feinberg School of Medicine
Northwestern University
Chicago, IL 60611, USA

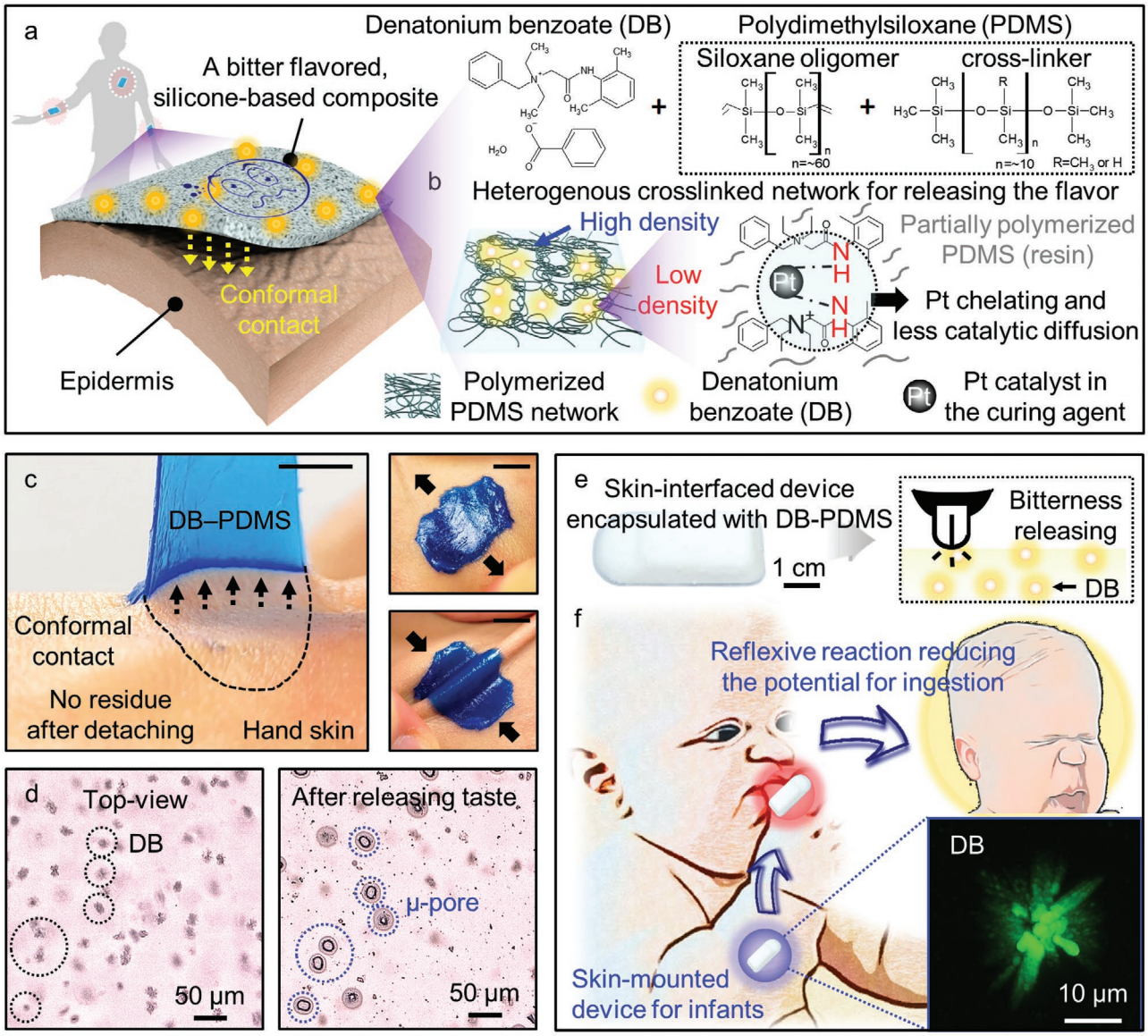

Figure 1. Design of a bitter-flavored, silicone composite as encapsulation and adhesive layers in skin-mounted devices. These systems minimize risks associated with choking when used with infants. a) Conceptual illustration of the DB-PDMS composite and b) material scheme that depicts the heterogeneity in the crosslinking network. c) Photographs of the DB-PDMS attached to the skin of the back of the hand under mechanical deformations. Inset scale bar: 1 cm. d) High-resolution digital image of the surface of a sample of the composite before (left) and after the water-induced dissolution of the DB near the surface (right). e) Demonstration of a skin-interfaced device encapsulated with DB-PDMS and f) schematic illustration of the safety aspect of this materials system, based on reflexive reactions that discourage ingestion. The inset is a 3D confocal fluorescence image of a microparticle of DB in the DB-PDMS composite.

Similar composites can be formed with conductive hydrogel adhesives (CHA), based on the 2-acrylamido-2- methylpropane sulfonic acid/acrylic acid (AMPS/AA) copolymer, including commercially available, FDA-approved materials (KM 40A, KATECHO).[32] The process in this case involves immersing the CHA in a solution of DB (22.4×10^{-3} M) for up to 60 min (Figure 2d). The inclusion of DB (446.6 g mol^{-1}) into the hydrogel matrix occurs via passive diffusion.[33–36] The doping time must be selected to achieve both mechanical stability of the DB-CHA and effective DB inclusion in the matrix (Figure S4, Supporting Information). The composite material (DB-CHA) that results from these doping procedures offers optical, mechanical, and electrical properties that are comparable to those of the undoped case. As shown in Figure 2e, the DB-CHA remains optically transparent in the visible range (>80% total transmittance, suitable for an optical interface to the skin). Compared to the non-doped CHA, the decrease in normal transmittance (e.g., 15.5% for 30 min doped DB-CHA and 63.2% for 60 min doped DB-CHA at 550 nm) can be explained by light scattering from DB microparticles that precipitate in the matrix during the drying step (Figure S5, Supporting Information), and do not fully dissolve during the rehydration process. Increasing

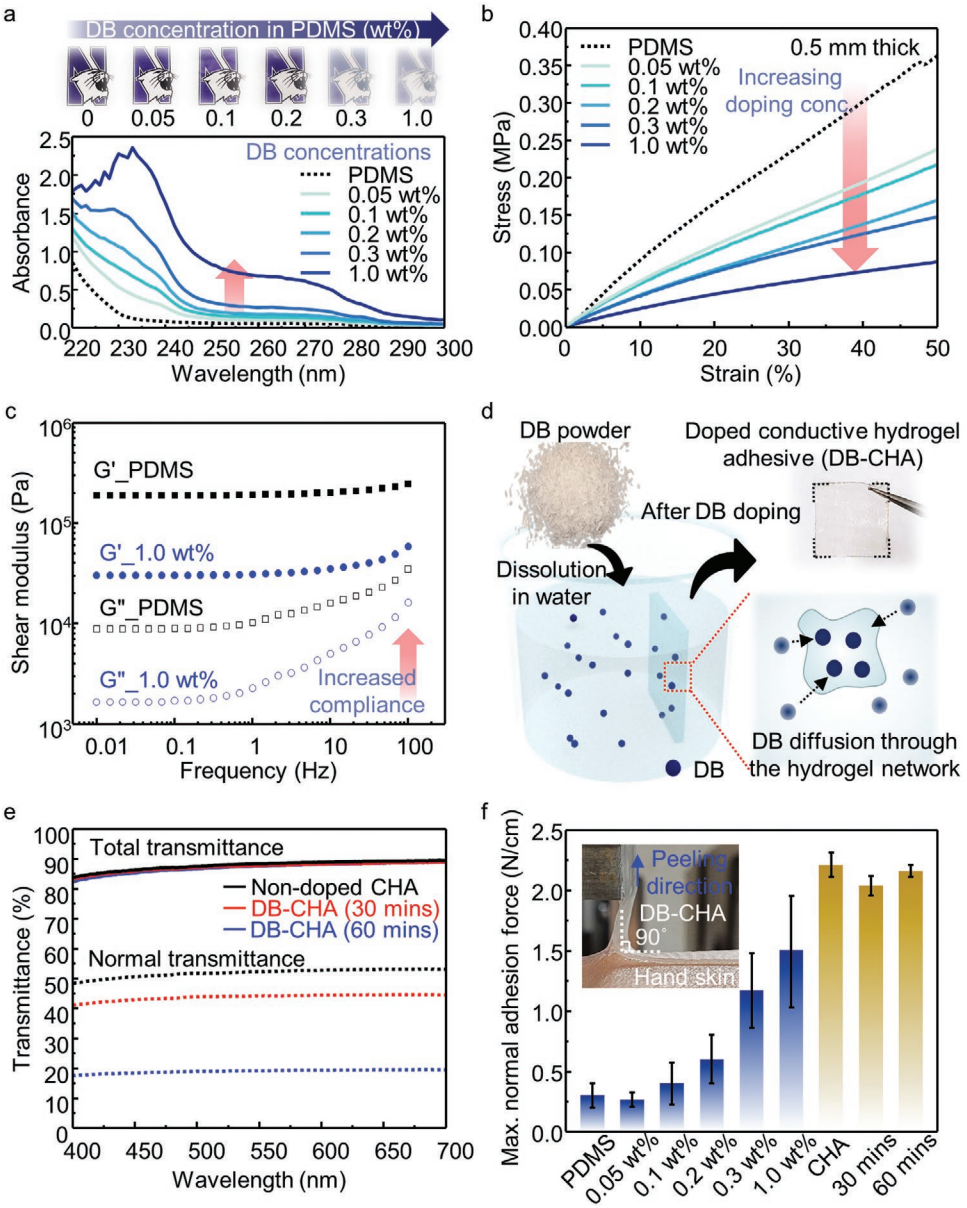

Figure 2. Optical and mechanical properties of DB-PDMS and DB-CHA composite materials. a) Images of films of DB-PDMS and their absorbance spectra measured using an integrating sphere. b) Stress–strain curves of DB-PDMS. c) Shear modulus of PDMS and DB-PDMS (1.0 wt%). d) Schematic illustrations of the fabrication procedures for DB-CHA, and an image of a sample. e) Transmittance of DB-CHA as a function of DB doping time. f) Maximum normal adhesion forces to the skin of the back of the hand for various materials.

the loading of DB by increasing the doping time increases the absorbance in the UV regime (Figure S6, Supporting Information). The mechanical properties of DB-CHA show some, relatively small, differences compared to those of non-doped CHA for strains up to 20% because of disentanglement of the AMPS/AA network by water permeation; the properties from 20% to 50% are similar (Figure S7, Supporting Information). The resistivity of this hydrogel is somewhat higher than that of typical commercial gels for electrical measurements on the skin (Figure S7, Supporting Information), but their gentle, skin-safe adhesion properties and their soft, elastic mechanics are essential characteristics for the applications considered here.

Measurements of the maximum normal force for peeling samples of these two types of composite materials (DB-PDMS and DB-CHA) from the skin of the hand define the adhesive characteristics relevant to their use in skin-interfaced devices. The DB-PDMS exhibits an adhesion force that increases monotonically with DB doping, consistent with corresponding reductions in the modulus and associated improvements in surface compliance (Figure 2f). Specifically, the adhesion force of the 1.0 wt% composite is ≈5 times higher (≈1.5 N cm^{-1}) than that of the pure PDMS (≈0.3 N cm^{-1}). By contrast, the DB-CHA shows no significant dependence of the adhesion on the doping level.

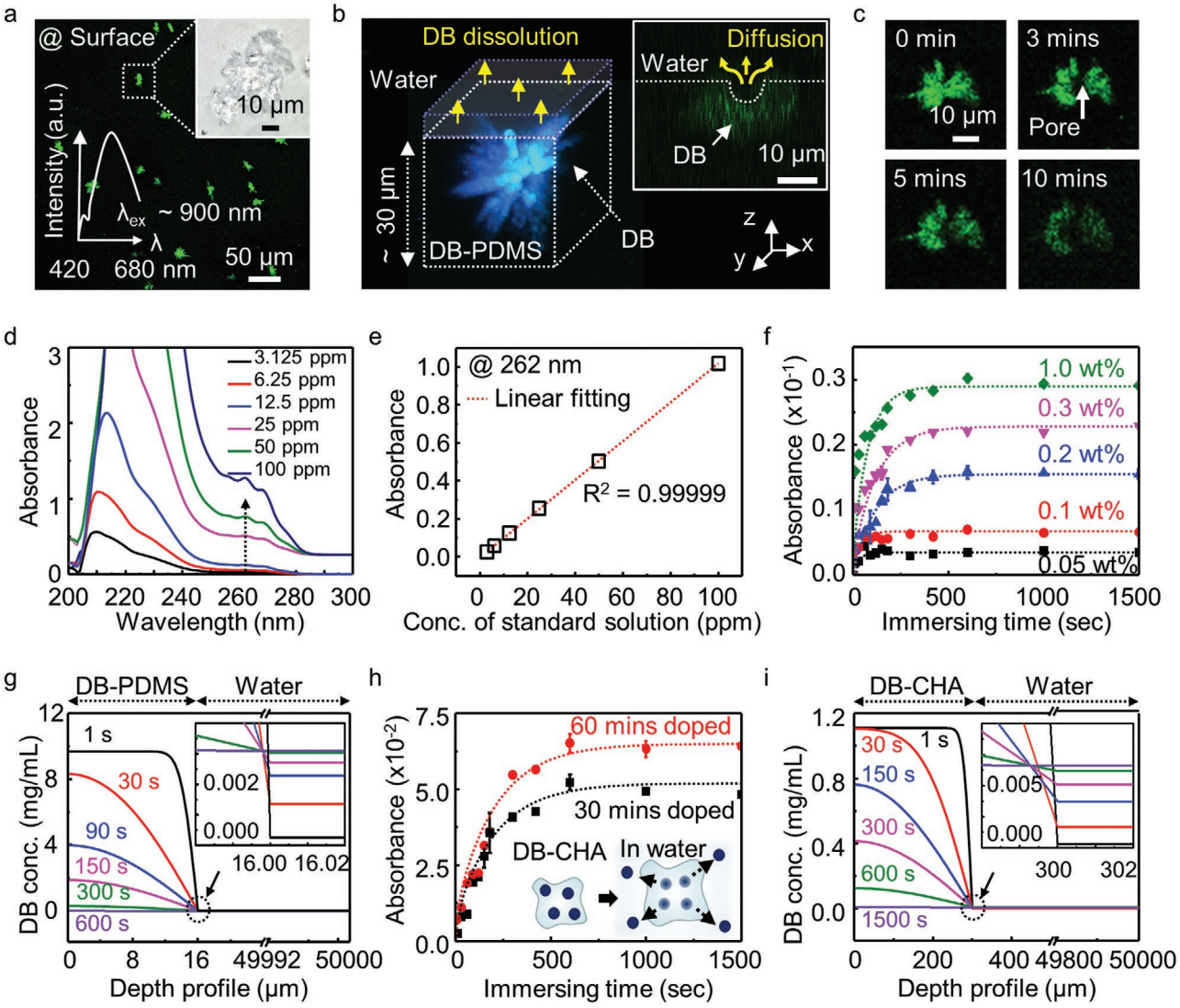

Figure 3. Morphological and quantitative analysis of DB-doped materials. a) Top-view confocal microscopy image of the DB-PDMS. The lower inset is the measured autofluorescence spectrum for DB under two photon excitation at a wavelength of 900 nm. b) 3D mapping of DB in the composite. The inset presents a cross-sectional view of the DB dissolving into water (at *XZ* plane). c) Top view of the time-dependent dissolution of DB into water. d) Absorbance spectra of DB standard solutions. e) Linear relation between the absorbance of the standard solutions at 262 nm and the DB concentration. f) Calculated (lines) and measured (dots) absorbance for DB-PDMS as a function of DB concentration and time of immersion in water. g) Computed dependence of the concentration of DB on depth in a 1.0 wt% DB-PDMS composite when immersed in water for t = 1, 30, 90, 150, 300, and 600 s. h) Calculated (lines) and measured (dots) absorbance at 262 nm for DB-CHAs formed by doping for 30 and 60 min. i) Computed dependence of the concentration of DB in a sample of DB-CHA doped for 60 min when immersed in water for t = 1, 30, 150, 300, 600, and 1500 s.

2.3. Diffusion Kinetics for Releasing the DB Bitterant

The key feature of these composites is their ability to release DB into an aqueous environment, including that associated with saliva in the mouth. The kinetics of the diffusive processes that govern this release depends on the distribution of the DB within the supporting matrix. 3D multiphoton microscopy based on the autofluorescence of DB (emission peak at 520 nm) under ≈900 nm excitation reveals this distribution for this case of DB-PDMS. Microparticles of DB (diameter ≈ 30 μm) appear not only at the surface but also into the depth of the composite, as might be expected (**Figure 3**a and Figure S8: Supporting Information). Immersion into water generates pores at the locations of these microparticles (Figure 3b). These pores gradually grow in size until they reach dimensions comparable to those of the microparticles (Figure 3c and Figure S9: Supporting Information). Dissolution occurs mostly in the near surface region, to define the release kinetics of the DB from the composite.

Concentration-dependent changes in the optical properties of the surrounding water provide a means for quantifying the release kinetics. Specifically, the UV absorbance values of DB standard solutions define a relationship between the absorbance and concentration, as shown for cases of 3.125, 6.25, 12.5, 25,

50, and 100 ppm in Figure 3d. Figure 3e and Figure S10 (Supporting Information) highlight a linear increase in absorbance with concentration at a wavelength of 262 nm, consistent with Beer's law, $A = \varepsilon lc$ where A is absorbance, ε is the molar extinction coefficient, l is the optical path length, c is the concentration (Figure S10, Supporting Information).[37] Values of absorbance of a volume of water measured before and after immersing/removing the sample in/out of the water thereby determine the amount of released DB (Figure S11, Supporting Information). The absorbance increases with DB doping up to 1.0 wt% (Figure 3f). The release process slows after ≈300 s for all cases.

The underlying physics can be captured with a 1D diffusion model, applicable because the thickness of the sample is much smaller than its length and width. Due to the symmetry of diffusion, a half system can be considered, with the origin o of the coordinate system located at the middle of the sample and the oy axis going along its thickness direction (Figure S12, Supporting Information). The equivalent half depth of water and the half effective releasing thickness of the sample are denoted by a and b, respectively. Introducing the mass of DB that remains in the sample per unit area between $y = 0$ and $y = y$ as $M(y,t) = \int_0^y w(\overline{y},t)\,\overline{d}y$, where the DB concentration w depends on both location y and time t, the diffusion theory yields the governing equation for M as $\frac{\partial M}{\partial t} = D\frac{\partial^2 M}{\partial y^2}(0 \le y < b)$, where D is the DB diffusivity (details appear in the experimental section). A constant initial DB concentration w_0 in the sample requires $M|_{t=0} = w_0 y$. Besides the boundary condition $M|_{y=0} = 0$, the conservation of the total mass of DB requires $M|_{y=b} + a\frac{\partial M}{\partial y}|_{y=b} = bw_0$ given the nearly uniform distribution of the released DB in water. By the method of variable separation, the analytical solution of the above governing equation with initial and boundary conditions is (details appear in the experimental section)

$$M(y,t) = aw_0\left\{\frac{by}{a(a+b)} + 2\sum_{n=1}^{\infty}\left[\frac{1}{\sin\xi_n - \xi_n\sec\xi_n}\sin\left(\frac{\xi_n y}{b}\right)\exp\left(-\frac{D\xi_n^2}{b^2}t\right)\right]\right\} \quad (1)$$

by which the mass of DB released in water is obtained as

$$M_{\text{released}} = aw_0 A\left\{\frac{b}{a+b} - 2\sum_{n=1}^{\infty}\left[\frac{\exp\left(-\frac{D\xi_n^2}{b^2}t\right)}{1 - \frac{2\xi_n}{\sin(2\xi_n)}}\right]\right\} \quad (2)$$

where A is the in-plane area of the sample. The DB concentration in the sample is obtained by the first-order derivative of M with respect to y:

$$w = w_0\left\{\frac{b}{a+b} - 2\sum_{n=1}^{\infty}\left[\frac{a}{a\cos\xi_n + b\sec\xi_n}\cos\left(\frac{\xi_n y}{b}\right)\exp\left(-\frac{D\xi_n^2}{b^2}t\right)\right]\right\} \quad (3)$$

Here, ξ_n are the positive roots of the transcendental equation $\tan(\xi_n) + \frac{a\xi_n}{b} = 0$ $(n = 1, 2, 3, \cdots)$.

The distribution of DB concentration along the thickness direction with 1.0 wt% DB-PDMS appears in Figure 3g for a time of immersion up to 600 s, as the most active release performance. The gradient of DB concentration in the sample decreases with time due to diffusion, achieving its maximum at the sample/water interface. A uniform distribution of DB concentration is eventually achieved after saturation, at the value $w = \frac{bw_0}{a+b}$ according to Equation (3). Specifically, the saturated DB concentrations are 0.59, 0.91, 1.8, 2.5, and 3.1 μg mL^{-1} (inset of Figure 3g) for the composites with 0.05, 0.1, 0.2, 0.3, and 1.0 wt% of DB, respectively and well-matched with the measured data.

The diffusion model also describes the kinetics of release from the DB-CHA system, which differs from the DB-PDMS in the effective thickness that participates in the release, defined by the measured amount of DB released in water at saturation. The DB-CHA engages the entire thickness of 600 μm (the half-effective releasing thickness is b = 300 μm) in the release process, due to the effective transport of water through the hydrogel network. As shown in Figure 3h, DB-CHA formed by doping for 30 min and 60 min (doping levels of 5.3 and 6.6 μg mL^{-1} respectively, based on measurements of UV absorbance in Figure 3h), show ≈70% and ≈110% improvements in the release performance, compared with the highest performance from the DB-PDMS (≈3 μg mL^{-1}), respectively.

The modeling results agree well with experimental measurements. The simulation spans ≈1500 s to reach saturation, although 600 s is sufficient to completely release the DB, as confirmed by the experimental results. This time for saturation is larger than that for the 1.0 wt% DB-PDMS because the effective thickness over which DB can be released from the DB-CHA system (full thickness, ≈600 μm) is much larger than that for the DB-PDMS (effective thickness of ≈16 μm). Figure 3i shows the distribution of DB along the thickness direction in the hydrogel system formed with 60 min doping as a function of the time of immersion (t = 1, 30, 150, 300, 600, and 1500 s). The concentrations saturate at 5.3 and 6.6 μg mL^{-1} for hydrogel samples doped for 30 and 60 min, respectively, consistent with experimental results in Figure 3h. Given a bitterness threshold of 0.05 ppm, the required time for a taste sensation is estimated to be 6.3 and 4.8 s for DB-PDMS and DB-CHA, respectively. The release kinetics in the short time regime are most important for the applications considered here.

2.4. Skin-Interfaced Biosensors Formed with Composite Materials That Reduce Choking Risks

Three representative skin-interfaced devices serve as the basis for demonstrating these composite materials in health monitoring applications of relevance to neonatal and pediatric patients: 1) a mechano-acoustic sensor for tracking motions and vibratory signatures of body processes (MA device),[5,38,39] 2) an electrocardiogram monitor for measuring cardiac health (ECG device),[40] and 3) a near-infrared spectroscopy device

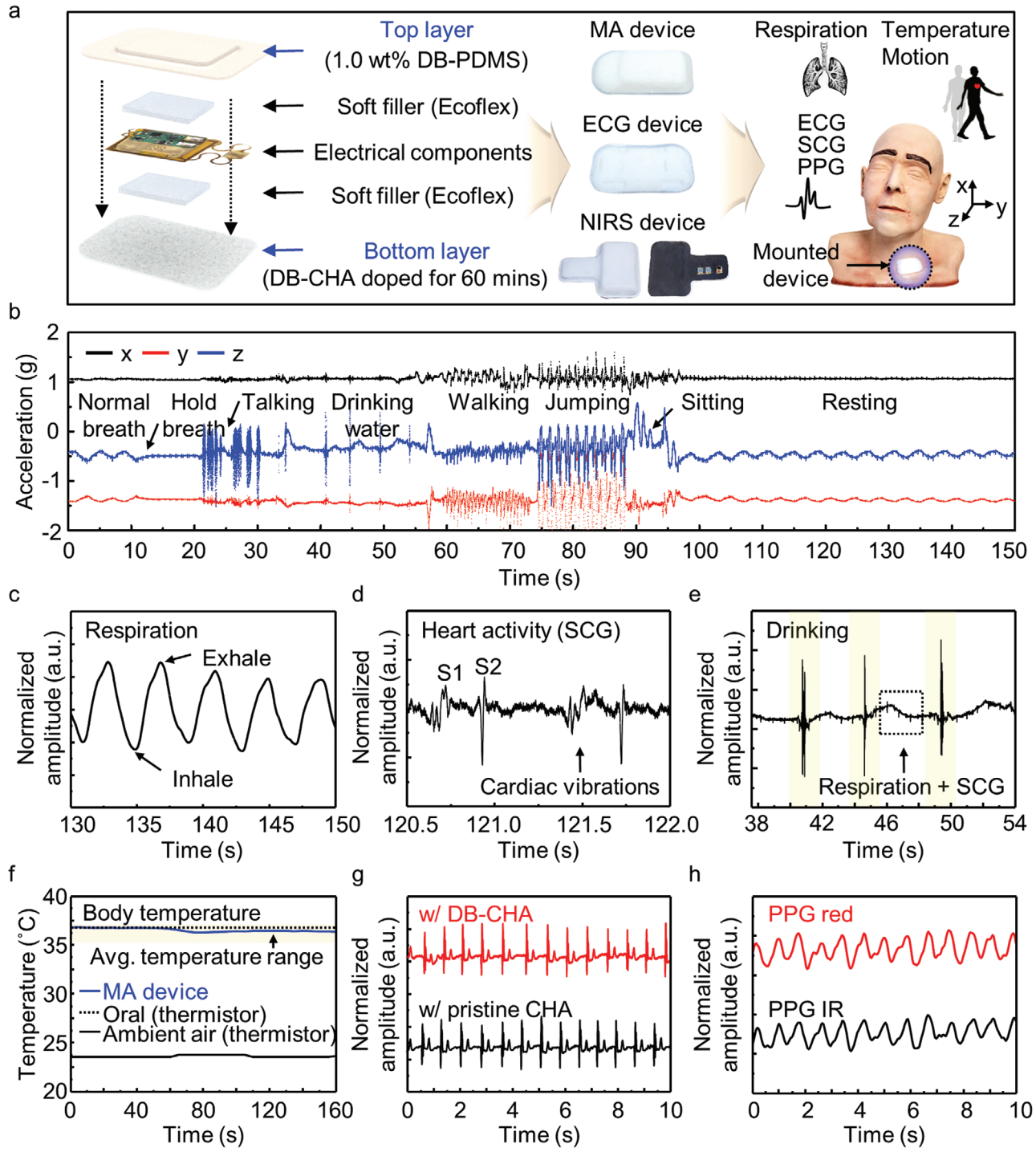

Figure 4. Skin-interfaced wireless health-monitoring devices that use bitterant-doped materials for encapsulation layers and adhesives, as safety features to prevent choking hazards when used with infants. a) Exploded view schematic illustrations of a device that uses a top encapsulating layer of 1.0 wt% DB-PDMS, over active electronic components (depending on the device type), soft fillers, and a bottom adhesive layer of DB-CHA (60 min doping time), and its application for measuring various vital signs. b) Three-axis accelerometry, as representative MA data recorded over a 150 s interval as a subject engages in various activities including talking, drinking, walking, jumping, and sitting at rest. c) Sample time-series data and spectrograms corresponding to respiration (c), cardiac activity (d), and drinking (e). f) Measurement of body temperature. g) Representative ECG waveforms and h) PPG red and PPG IR signals, collected from the ECG monitoring device and NIRS device coupled with DB-CHA adhesive, respectively.

for capturing signatures of cerebral hemodynamics (NIRS device).[41] The composite, bitter-tasting materials serve as soft encapsulants and/or skin adhesives for these systems. **Figure 4**a shows an exploded-view illustration of a representative example.

Here, the DB-PDMS with 1.0 wt% encapsulates the electronics and the DB-CHA (60 min doped) provides an electrically conductive, transparent adhesive interface to the skin. In the first example, an MA device prepared in this fashion mounts on the suprasternal notch (SN) to yield time series data related to diverse physiological processes and core-body motions,[40] in the form of 3-axis, wide bandwidth accelerometry, and temperature sensing. Data from a healthy subject participating in a series of activities appears in Figure 4b. The features include respiratory behaviors and cardiac sounds. Accelerations in the direction perpendicular to the surface of the skin show repeated expansion and contraction of the chest wall, highlighted by normal breathing during the first 10 s of the data. After a breath hold that extends for a following 10 s, the subject engages in talking and drinking to create data features that correspond to acoustic vibrations and rapid motions. Subsequent, large-amplitude accelerations with significant projections along all axes follow from periods of walking (59–72 s), jumping (74–88 s), and sitting (89–96 s), followed by recovery to the original stationary state, with controlled respirations. The quality of data captured with these devices is identical to that associated with devices that use conventional encapsulants and adhesives (Figure 4c–f). A bilayer of DB-PDMS (1.0 wt%) and undoped PDMS can also be considered as the encapsulant. Due to the good adhesion at the interface between these materials (Figure S13, Supporting Information), the physical properties of a conventional PDMS based encapsulating structure are only slightly modified by the presence of the DB-PDMS coating.

The conductivity of the DB-CHA enables measurements of ECGs. For this demonstration, an ECG device encapsulated with DB-PDMS couples to the skin with the DB-CHA to yield clean waveforms with distinctly separated P, QRS, and T features. These signals are comparable to those obtained with undoped CHA (Figure 4g). The optical transparency of DB-CHA enables the operation of the NIRS device for measuring reflectance-mode photoplethysmograms (PPGs) based on operation at red (740 nm) and infrared (IR, 850 nm) wavelengths, sampled at 25 Hz (Figure 4h).

3. Conclusion

We have demonstrates that a harmless bitterant can be introduced into soft matrix materials to yield encapsulation layers and gentle adhesives for advanced, miniaturized wearable devices designed to minimize choking hazards when used with infants. A comprehensive set of experimental and modeling results define the structure/property relationships in these unusual composites. This materials strategy provides a means for introducing bitter taste into silicone materials and, at the same time, for tuning the volumetric density of crosslinks and associated physical properties. The result is a composite with broad utility as an encapsulating or interfacial adhesive material across a range of skin-mounted device technologies, with an important safety feature against ingestion. This work demonstrates the first of many opportunities where advanced materials can contribute to enhanced safety in skin-integrated health monitoring devices, with applications that span all age groups and application scenarios.

4. Experimental Section

Fabrication of DB-PDMS: The process began with micro-ball milling of denatonium benzoate powder (>98%, Sigma) using stabilized zirconia balls (diameter of 0.3–0.4 mm and 1.4–1.7 mm) in a planetary mixer (ARE-310, Thinky) for 5 min at 2000 rpm. Subsequently, the pulverized powders passed through two microsieves (100 mesh from Talisman and US2.5-325B standard brass sieve from Dual manufacturing Co., Inc.) to collect fine powders of microparticles with diameters of less than 45 µm. Formation of the DB-PDMS involved adding DB powder into a base polymer precursor (Sylgard 184, Dow Corning) and mixing thoroughly in a planetary mixer for 30 s at 2000 rpm and degassing 30 s at 2200 rpm. A PDMS curing agent (Sylgard 184, Dow Corning) introduced into the mixture (10:1 ratio of the base and curing agent) preceded another cycle of mixing for 30 s at 2000 rpm and degassing 30 s at 2200 rpm. The resulting mixture of DB powder and PDMS was then poured into a petri dish substrate. Additional degassing occurred by placing the sample in a vacuum chamber for 1 h, prior to thermal curing at 75 °C for 2–3 h.

Fabrication of DB-CHA: A commercially available conductive hydrogel adhesive (KATECHO, KM 40A Hydrogel) served as a matrix for doping with DB. The first step in the process involved preparing a DB solution at a concentration of 22.4×10^{-3} M by adding DB to deionized water and then immersing the hydrogel in the solution (for 30 and 60 min for each case) after removing the liner (medium-density polyethylene) that accompanies the commercial product. Drying the material and then rehydrating it returns the hydrogel to its original state.

Diffusion Model for Release of DB: The governing equation for diffusion is

$$\frac{\partial w}{\partial t} = D\frac{\partial^2 w}{\partial y^2}(0 \le y < b) \tag{4}$$

A constant initial DB concentration w_0 in the sample and zero DB flux at the middle of the sample yield the following initial and boundary conditions:

$$w|_{t=0} = w_0(0 \le y < b) \tag{5}$$

$$\frac{\partial w}{\partial y}|_{y=0} = 0 \tag{6}$$

For the mass of DB that remains in the sample per unit area between $y = 0$ and $y = y$ defined as $M(y,t) = \int_0^y w(\bar{y},t)\bar{d}y$, integration of both sides of Equation (4) over (0, y) yields $\frac{\partial M}{\partial t} = D\left(\frac{\partial w}{\partial y} - \frac{\partial w}{\partial y}|_{y=0}\right)$, which, together with boundary condition in Equation (6) and $\frac{\partial^2 M}{\partial y^2} = \frac{\partial w}{\partial y}$, give

$$\frac{\partial M}{\partial t} = D\frac{\partial^2 M}{\partial y^2}(0 \le y < b) \tag{7}$$

The initial condition, boundary condition, and conservation of the total amount of DB require

$$M|_{t=0} = w_0 y(0 \le y < b)\, M|_{y=0} = 0 M|_{y=b} + a\frac{\partial M}{\partial y}|_{y=b} = bw_0 \tag{8}$$

in view of the instant uniform distribution of the released DB in water.

The following function is introduced

$$f(y,t) = M(y,t) - \frac{bw_0}{a+b}y \tag{9}$$

such that its governing equation and boundary conditions are all homogeneous

$$\frac{\partial f}{\partial t} = D\frac{\partial^2 f}{\partial y^2}(0 \le y < b) \tag{10}$$

$$f|_{t=0} = w_0 y - \frac{bw_0}{a+b}y(0 \le y < b) \tag{11}$$

$$f|_{y=0}=0 \tag{12}$$

$$f|_{y=b}+a\frac{\partial f}{\partial y}|_{y=b}=0 \tag{13}$$

The method of separation of variables, $f = Y(y)T(t)$ yields $D\frac{Y''}{Y}=\frac{T'}{T}=-\lambda$, with λ as the positive eigenvalue. The solutions are $T = \exp(-\lambda t)$ and $T = \exp(-\lambda t)$, where E, and F are the constants to be determined. The homogeneous conditions in Equations (12) and (13) require $F = 0$ and $\sin\left(b\sqrt{\frac{\lambda}{D}}\right)+a\sqrt{\frac{\lambda}{D}}\cos\left(b\sqrt{\frac{\lambda}{D}}\right)=0$ since E cannot be zero. The eigenvalues are thus the positive roots of the following transcendental equation:

$$\tan(\xi_n)+\frac{a}{b}\xi_n=0 \quad (n=1,2,3,\ldots) \tag{14}$$

where $\xi_n=b\sqrt{\frac{\lambda_n}{D}}$. Therefore, the general solution of f is $f=\sum_{n=1}^{\infty}\left[C_n\exp\left(-\frac{D\xi_n^2 t}{b^2}\right)\sin\left(\frac{\xi_n y}{b}\right)\right]$, with constants C_n to be determined from the initial condition in Equation (11), $\sum_{n=1}^{\infty}\left[C_n\sin\right)\left(\frac{\xi_n y}{b}\right)\Big]=\frac{aw_0 y}{(a+b)}$. The orthogonality of the eigenfunctions $\int_0^b\sin\left(\frac{\xi_m y}{b}\right)\sin\left(\frac{\xi_m y}{b}\right)dy=0 \quad (m\neq n)$ then gives $C_n=\frac{2aw_0}{(\sin\xi_n-\xi_n\sec\xi_n)}$. The final solution of f is

$$f=2aw_0\sum_{n=1}^{\infty}\left[\frac{1}{\sin\xi_n-\xi_n\sec\xi_n}\sin\left(\frac{\xi_n y}{b}\right)\exp\left(-\frac{D\xi_n^2}{b^2}t\right)\right] \tag{15}$$

The analytical solution of M is obtained as Equation (1) according to Equation (9). The mass of DB released in water is obtained by $M_{released} = A[bw_0 - M(b, t)]$, which yields Equation (2).

In the present study, all samples have the same length and width (≈1 cm) and the volume of water for immersion is 10 mL, such that the area $A = 1$ cm^2 and the equivalent depth of water $a = 5$ cm are used in the model. For the DB-PDMS, the surface localized effective thickness is offered for the release, as defined by the measured amount of DB released in water when the saturation is reached. Specifically, b = 61, 47, 46, 43, and 16 μm are adopted for the composite models and w_0 = 0.48, 0.97, 1.9, 2.9, and 9.7 mg mL^{-1} for the initial DB concentrations in the samples with 0.05, 0.1, 0.2, 0.3, and 1.0 wt% of DB, respectively. Based on the measured linearity between the absorbance and the concentration, it is noted that the DB concentration (X) in water (μg mL^{-1}) is related to the absorbance (Y) at 262 nm by $Y = 0.0102X - 0.00254$, which has been used in the modeling. Accordingly, the DB diffusivities in the matrix can be extracted using the present model as $D = 6 \times 10^{-11}$, 2.5×10^{-11}, 7×10^{-12}, 6×10^{-12}, and 1.3×10^{-12} m^2 s^{-1} for the composites with 0.05, 0.1, 0.2, 0.3, and 1.0 wt% of DB, respectively. Likewise, the initial DB concentrations in the doped hydrogel systems are determined to be w_0 = 0.90 and 1.1 mg mL^{-1} for DB-CHAs doped for 30- and 60-min and the DB diffusivity is also obtained as $D = 1.7 \times 10^{-10}$m^2 s^{-1}.

Assembly of the Device: Details of the fabrication methods for each type of skin-interfaced device and its data collections appear elsewhere.[5,40,41] The encapsulating structures adopted shapes defined by aluminum molds formed in geometries by design drawings (Solidworks) and a three-axis milling machine (Roland MDX 540). The top-encapsulating layer was prepared by casting the DB-PDMS (1.0 wt%) into the gap (thickness 300 μm) formed by aligned pairs of such molds. After curing in an oven at 75 °C for 3 h, the top layer was carefully peeled from the mold. A planar silicone substrate film enclosed the electronics by bonding to the top layer. The mold facilitated alignment with the substrate film and supported electronics. A silicone thermoset polymer (Ecoflex, 00–30, smooth-on) filled the air cavity that enclosed the electronics, cured at 75 °C in an oven for 15 min. A layer of DB-CHA (60 min doped) served as a soft, double-sided adhesive, conductive skin interface.

Characterizations: The DB-PDMS morphologies were characterized using a high-resolution digital microscope (VHX-1000 Keyence). The absorbance measurements were recorded using a UV-Vis spectrophotometer (Perkin Elmer LAMDA 1050). An integrating sphere module enabled measurements of the total absorbance. Mechanical tensile tests used a commercial instrument (TA instruments RSA G2). The sample dimensions were 10 mm wide, 20 mm long, and 500 μm thick. The shear and loss moduli of the DB-PDMS were measured using an automatic rheometer (Anton Paar MCR302), from 10^{-2} to 10^2 Hz with a constant interval depending on sample thickness, and a controlled force normal to the sample in a parallel plate geometry with 8 mm diameter at 25°C. The sample thickness was 700 μm and the applied strain was 0.5%. Adhesion tests used a digital force sensor (FGJN-5B, Shimpo). A commercial adhesive (3M) placed on the back sides of the samples eliminated contributions from elastic stretching of the samples during these measurements. Tests with human subjects used devices adhered to the skin of the backside of the hand with one end of the sample secured by a metallic clamp. The sample width and length were 10 and 20 mm, respectively. The peeling speed was 10 mm s^{-1} and the maximum adhesion force was determined during the peeling process. The electrical impedance of the DB-CHA was measured by using a polysomnography system (NicoletOne v44, Natus). 3D images of DB were captured with a confocal microscope (Nikon A1R-MP). For human subject studies, the studies were approved by the Northwestern University Institutional Review Board, Chicago, IL, USA (STU00202449 and STU00212522) and were registered on ClinicalTrials.gov (NCT02865070 and NCT04393558). The subjects took part following informed consent or following informed consent of a legal guardian or parent.

Supporting Information

Supporting Information is available from the Wiley Online Library or from the author.

Acknowledgements

D.C. and R.L. contributed equally to this work. R.L. gratefully acknowledges the support from the National Natural Science Foundation of China (grants 12022209 and 11972103) and Liaoning Revitalization Talents Program (grant XLYC1807126). The work was supported by the Querrey/Simpson Institute for Bioelectronics at Northwestern University.

Conflict of Interest

The authors declare no conflict of interest.

Data Availability Statement

The data that support the findings of this study are available from the corresponding author upon reasonable request.

Keywords

denatonium benzoate, safety materials, skin-interfaced wearables, soft electronics

Received: May 21, 2021
Revised: June 15, 2021
Published online: August 8, 2021

[1] H. Jeong, J. Y. Lee, K. Lee, Y. J. Kang, J.-T. Kim, R. Avila, A. Tzavelis, J. Kim, H. Ryu, S. S. Kwak, J. U. Kim, A. Banks, H. Jang, J.-K. Chang, S. Li, C. K. Mummidisetty, Y. Park, S. Nappi, K. S. Chun, Y. J. Lee, K. Kwon, X. Ni, H. U. Chung, H. Luan, J.-H. Kim, C. Wu, S. Xu, A. Banks, A. Jayaraman, Y. Huang, J. A. Rogers, *Sci. Adv.* **2021**, *7*, eabg3092.
[2] X. Ni, W. Ouyang, H. Jeong, J.-T. Kim, A. Tzaveils, A. Mirzazadeh, C. Wu, J. Y. Lee, M. Keller, C. K. Mummidisetty, M. Patel, N. Shawen, J. Huang, H. Chen, S. Ravi, J.-K. Chang, K. Lee, Y. Wu, F. Lie, Y. J. Kang, J. U. Kim, L. P. Chamorro, A. R. Banks, A. Bharat, A. Jayaraman, S. Xu, J. A. Rogers, *Proc. Natl. Acad. Sci. USA* **2021**, *118*, 2026610118.
[3] O. Bonner, K. Beardsall, N. Crilly, J. Lasenby, *BMJ Innovations* **2017**, *3*, 12.
[4] D. Cho, J. Park, J. Kim, T. Kim, J. Kim, I. Park, S. Jeon, *ACS Appl. Mater. Interfaces* **2017**, *9*, 17369.
[5] H. U. Chung, A. Y. Rwei, A. Hourlier-Fargette, S. Xu, K. Lee, E. C. Dunne, Z. Xie, C. Liu, A. Carlini, D. H. Kim, D. Ryu, E. Kulikova, J. Cao, I. C. Odland, K. B. Fields, B. Hopkins, A. Banks, C. Ogle, D. Grande, J. B. Park, J. Kim, M. Irie, H. Jang, J. Lee, Y. Park, J. Kim, H. H. Jo, H. Hahm, R. Avila, Y. Xu, M. Namkoong, J. W. Kwak, E. Suen, M. A. Paulus, R. J. Kim, B. V. Parsons, K. A. Human, S. S. Kim, M. Patel, W. Reuther, H. S. Kim, S. H. Lee, J. D. Leedle, Y. Yun, S. Rigali, T. Son, I. Jung, H. Arafa1, V. R. Soundararajan, A. Ollech, A. Shukla, A. Bradley, M. Schau, C. M. Rand, L. E. Marsillio, Z. L. Harris, Y. Huang, A. Hamvas, A. S. Paller, D. E. Weese-Mayer, J. Lee, J. A. Rogers, *Nat. Med.* **2020**, *26*, 418.
[6] H. Jeong, J. A. Rogers, S. Xu, *Sci. Adv.* **2020**, *6*, eabd4794.
[7] J. Xu, S. L. Murphy, K. D. Kochanek, B. Bastian, E. Arias, *Natl. Vital Stat. Rep.* **2018**, *67*, 1.
[8] K. Kim, B. Kim, C. H. Lee, *Adv. Mater.* **2020**, *32*, 1902051.
[9] T. Ray, J. Choi, J. Reeder, S. P. Lee, A. J. Aranyosi, R. Ghaffari, J. A. Rogers, *Curr. Opin. Biomed. Eng.* **2019**, *9*, 47.
[10] C. Xu, Y. Yang, W. Gao, *Matter* **2020**, *2*, 1414.
[11] B. G. Nichols, A. Visotcky, M. Aberger, N. M. Braun, R. Shah, S. Tarima, D. J. Brown, *Int. J. Pediatr. Otorhinolaryngol.* **2012**, *76*, 169.
[12] D. S. Sundari, D. V. Rajeswari, *Eur. J. Mol. Clin. Med.* **2021**, *7*, 5986.
[13] G. P. Digoy, *Otolaryngol. Clin. North Am.* **2008**, *41*, 485.
[14] R. Higo, Y. Matsumoto, K. Ichimura, K. Kaga, *Auris Nasus Larynx* **2003**, *30*, 397.
[15] P. S. Lemberg, D. H. Darrow, L. D. Holinger, *Ann. Otol. Rhinol. Laryngol.* **1996**, *105*, 267.
[16] R. Sethia, H. Gibbs, I. N. Jacobs, J. S. Reilly, K. Rhoades, K. R. Jatana, *Laryngoscope Investig. Otolaryngol.* **1996**, *105*, 267.
[17] Nintendo, https://www.nintendo.co.uk/Support/Nintendo-Switch/FAQ/After-touching-a-Nintendo-Switch-game-card-my-hand-has-a-strange-bitter-taste-Could-this-be-harmful-/After-touching-a-Nintendo-Switch-game-card-my-hand-has-a-strange-bitter-taste-Could-this-be-harmful--1204008.html, (accessed: May 2021).
[18] C. K. Berning, J. F. Griffith, J. E. Wild, *Fundam. Appl. Toxicol.* **1982**, *2*, 44.
[19] H. Payne, H. Smalley, M. Tracy, *SAE Tech. Pap.* **1993**, *930589*, 9.
[20] U.S. Consumer Product Safety Commission. U.S. Consumer Product Safety Commission CPSC **1997**, https://web.archive.org/web/20110616104140/http://www.cpsc.gov/LIBRARY/FOIA/foia99/os/aversive.pdf (accessed: May 2021).
[21] C. F. Carlborg, T. Haraldsson, M. Cornaglia, G. Stemme, W. van der Wijngaart, *J. Microelectromech. Syst.* **2010**, *19*, 1050.
[22] S. H. Jeong, S. Zhang, K. Hjort, J. Hilborn, Z. Wu, *Adv. Mater.* **2016**, *28*, 5830.
[23] Y. Xia, G. M. Whitesides, *Annu. Rev. Mater. Sci.* **1998**, *28*, 153.
[24] Z. Anfar, A. Amedlous, M. Majdoub, A. A. El Fakir, M. Zbair, H. A. Ahsaine, A. Jada, N. El Alem, *RSC Adv.* **2020**, *10*, 31087.
[25] R. W. Style, R. Boltyanskiy, B. Allen, K. E. Jensen, H. P. Foote, J. S. Wettlaufer, E. R. Dufresne, *Nat. Phys.* **2015**, *11*, 82.
[26] F. Di Lorenzo, S. Seiffert, *Polym. Chem.* **2015**, *6*, 5515.
[27] G. S. Crosson, K. M. Crosson, S. Thorpe, L. MacPherson, M. Murdock, B. Smith, *J. Water Resour. Prot.* **2014**, *6*, 793.
[28] K. Raman, T. S. Murthy, G. Hegde, *Phys. Procedia* **2011**, *19*, 146.
[29] D. Cho, Y. S. Shim, J. W. Jung, S. H. Nam, S. Min, S. E. Lee, Y. Ham, K. Lee, J. Park, J. Shin, S. Jeon, *Adv. Sci.* **2020**, *7*, 1903708.
[30] B. Pranaitytė, Z. Daunoravicius, A. Padarauskas, *Chromatographia* **2004**, *60*, 353.
[31] T. Kim, J. Park, J. Sohn, D. Cho, S. Jeon, *ACS Nano* **2016**, *10*, 4770.
[32] C. Liu, J. T. Kim, S. S. Kwak, A. Hourlier-Fargette, R. Avila, J. Vogl, A. Tzavelis, H. U. Chung, J. Y. Lee, D. H. Kim, D. Ryu, K. B. Fields, J. L. Ciatti, S. Li, M. Irie, A. Bradley, A. Shukla, J. Chavez, E. C. Dunne, S. S. Kim, J. Kim, J. B. Park, H. H. Jo, J. Kim, M. C. Johnson, J. W. Kwak, S. R. Madhvapathy, S. Xu, C. M. Rand, L. E. Marsillio, S. J. Hong, Y. Huang, D. E. Weese-Mayer, J. A. Rogers, *Adv. Healthcare Mater.*, https://doi.org/10.1002/adhm.202100383.
[33] Z. Ma, W. Shi, K. Yan, L. Pan, G. Yu, *Chem. Sci.* **2019**, *10*, 6232.
[34] O. Okay, in *Hydrogel Sensors and Actuators*, Springer, New York **2009**, p. 1.
[35] Y. Fu, W. J. Kao, *Expert Opin. Drug Delivery* **2010**, *7*, 429.
[36] B. Björkner, *Contact Dermatitis* **1980**, *6*, 466.
[37] T. G. Mayerhöfer, J. Popp, *ChemPhysChem* **2019**, *20*, 511.
[38] S. Xu, A. Y. Rwei, B. Vwalika, M. P. Chisembele, J. S. Stringer, A. S. Ginsburg, J. A. Rogers, *Lancet Digital Health* **2021**, *3*, 266.
[39] L. Lonini, N. Shawen, O. Botonis, M. Fanton, C. Jayaraman, C. K. Mummidisetty, S. Y. Shin, C. Rushin, S. Jenz, S. Xu, *IEEE J. Transl. Eng. Health Med.* **2021**, *9*, 4900311.
[40] K. Lee, X. Ni, J. Y. Lee, H. Arafa, J. P. David, S. Xu, R. Avila, M. Irie, J. H. Lee, R. L. Easterlin, D. H. Kim, H. U. Chung, O. O. Olabisi, S. Getaneh, E. Chung, M. Hill, J. Bell, H. Jang, C. Liu, J. B. Park, J. Kim, S. B. Kim, S. Mehta, M. Pharr, A. Tzavelis, J. T. Reeder, I. Huang, Y. Deng, Z. Xie, C. R. Davies, Y. Huang, J. A. Rogers, *Nat. Biomed. Eng.* **2020**, *4*, 148.
[41] A. Y. Rwei, W. Lu, C. Wu, K. Human, E. Suen, D. Franklin, M. Fabiani, G. Gratton, Z. Xie, Y. Deng, S. S. Kwak, L. Li, C. Gu, A. Liu, C. M. Rand, T. M. Stewart, Y. Huang, D. E. Weese-Mayer, J. A. Rogers, *Proc. Natl. Acad. Sci. USA* **2020**, *117*, 31674.